Inorganic Chemistry

Article

pubs.acs.org/IC

New $[PbBi_2O_4][Bi_2O_2]Cl_2$ and $[Pb_nBi_{10-n}O_{13}][Bi_2O_2]_nCl_{4+n}$ Series by Association of Sizable Subunits: Relationship with Arppe's Compound $Bi_{24}O_{31}Cl_{10}$ and Luminescence Properties

A. Aliev,[†] J. Olchowka,[†,‡] M. Colmont,[†] E. Capoen,[†] C. Wickleder,[‡] and O. Mentré*[,†]

[†]Université Lille Nord de France, UMR 8181 CNRS, Unité de Catalyse et de Chimie du Solide (UCCS USTL), F-59655 Villeneuve d'Ascq, France

[‡]Inorganic Chemistry, Faculty for Science and Technology, University of Siegen, 57068 Siegen, Germany

Supporting Information

ABSTRACT: Four new mixed lead–bismuth oxychloride compounds have been prepared and characterized by single crystal X-ray diffraction. Their crystal structures are described on the basis of the association of distinct building units found in parent Pb or Bi oxychlorides. The new compound $PbBi_4O_6Cl_2$ is formed of the stacking of 2D positive $[Bi_2O_2]^{2+}$ layers and neutral $[PbBi_2O_4]^0$ double layers separated by Cl^- anions. Similar motifs with finite lengths are combined together in the new series $[Pb_nBi_{10-n}O_{13}]$-$[Bi_2O_2]_nCl_{4+n}$. From the structural viewpoint, it is striking that this family of homologous phases is strongly related to $Bi_{24}O_{31}Cl_{10}$ well-known as Arppe's compound in which the fluorite-like $[Bi_2O_2]_n$ subunit was increased from $n = 1$ (mixed Bi/Pb Arppe's compound) to $n = 2$, 3, and 4 new members. The preparation of the respective powders shows the predominant stability of the $n = 2$ term which was prepared as a single-phase, while other terms have not been obtained in absence of secondary phases. For $n = 2$, the impedance spectroscopy shows a conductivity value $\sigma \sim 10^{-3}$ S cm^{-1} at 650 °C and suggests a contribution of Cl^- in the diffusion process. Most remarkable, $PbBi_4O_6Cl_2$ as well as $[Pb_2Bi_8O_{13}][Bi_2O_2]_2Cl_6$ show very bright red emission at low temperature, which could be assigned to Bi^{3+} transitions by comparison to $BaBi_4O_6Cl_2$. The different shapes of the excitation spectra lead to the assumption of a complete Pb–Bi energy transfer.

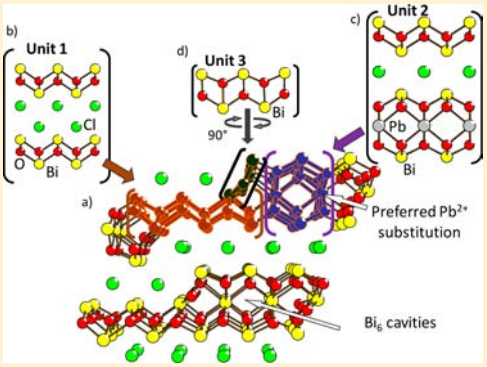

INTRODUCTION

In addition to their structural versatility and adaptability into various layered topologies, metal oxyhalides are of general interest since they exhibit several interesting properties including luminescence[1] and selective oxidation catalysis.[2] Recently, Sillen-Aurivillius intergrowths phases $Bi_6Ti_2MO_{14}Cl$ (M^{3+} = Cr^{3+}, Mn^{3+}, or Fe^{3+}) have been announced as good templates for naturally layered multiferroics and at least display ferroelectric properties.[3] The recently discovered $BiO(IO_3)$ displays good second harmonic generation properties due to its noncentrosymmetric space group[4] due to iodate groups replacing halides in the parent BiOCl compound. Related compounds with nitrate groups in the interleave broaden the domain of existence of such layered bismuth based compounds.[5] Due to this rich playground concomitant with our current interest in the design by a rational approach of new Bi-based compounds,[6,7] we focus on new topologies of layered bismuth-based oxyhalides compounds.

The richness of the crystal chemistry of bismuth oxides and salts is governed not only by the distorted geometry of coordination of Bi^{3+} due to its stereoactive $6s^2$ lone pair[8] but also by its ability for creating building units made of oxo-centered OBi_n polyhedra.[9] Typically, fluorite-type $[Bi_2O_2]^{2+}$ layers are formed by edge-sharing OBi_4 tetrahedra. The compound $Bi_{24}O_{31}Cl_{10}$ (also known as "Arppe's compound") is a product of the thermal decomposition of BiOCl, which has been known since 1845.[10] It is formed of rarely observed crenel-like 2D-layers of OBi_4 tetrahedra separated by single Cl^- layers. Its crystal structure was first resolved by Sillen and Edstrand in 1942,[11] while it was revised in doubled unit cell in 2000.[12] Here we present a novel homologous series related to the original Arppe's compound by modification of the topology of the crenel-layers by incorporation of Pb^{2+} cations with the general formula $[Pb_nBi_{10-n}O_{13}][Bi_2O_2]_nCl_{4+n}$ (n = 1, 2, 3, and 4) and related compound $[PbBi_2O_4][Bi_2O_2]Cl_2$ (=$PbBi_4O_6Cl_2$).

The choice of Pb^{2+} as the substituent for Bi^{3+} naturally follows from their aliovalent but iso-electronic character, and because the former also exhibits plethora of oxohalides synthetic structures.[13,14] They are also encountered as minerals for example mendipite $Pb_3O_2Cl_2$[15] and can show good ionic conductivity due to the disorder in the chlorine layers.[16] More generally mixed Bi/Pb compounds of the BiOCl–$PbCl_2$ system shows an array of layered phases depending on the Bi/Pb

Received: February 4, 2013
Published: July 24, 2013

   dx.doi.org/10.1021/ic4002708 | Inorg. Chem. 2013, 52, 8427–8435

Table 1. Conditions and Results of the Attempts to Reproduce the Compounds in the Form of Powder[a]

formulation	formula	T, °C	conditions	phase found
n = 1				
$Pb_nBi_{10-n}O_{13}[Bi_2O_2]_nCl_{4+n}$	$Bi_9PbO_{13}[Bi_2O_2]Cl_5$	750	sealed tube	n = 2 + weak amount u.p.
	$Bi_9PbO_{13}[Bi_2O_2]Cl_5$	730, 750	air	n = 1 + $Bi_{24}O_{31}Cl_{10}$ + u.p.
slight chemical deviation from formulation	$Bi_{9.5}Pb_{0.5}O_{13.25}[Bi_2O_2]Cl_5$	800	sealed tube	n = 1 + n = 2 + $Bi_{24}O_{31}Cl_{10}$ + u.p.
	$Bi_{9.66}Pb_{0.34}O_{13}[Bi_2O_2]Cl_5$	700, 720	air	n = 1 + $Bi_{24}O_{31}Cl_{10}$ + Bi_3O_4Cl
n = 2				
$Pb_nBi_{10-n}O_{13}[Bi_2O_2]_nCl_{4+n}$	$Bi_8Pb_2O_{13}[Bi_2O_2]_2Cl_6$	750	sealed tube	n = 2 single phase
slight chemical deviation from formulation	$Bi_{8.5}Pb_{1.5}O_{13.25}[Bi_2O_2]_2Cl_6$	800	sealed tube	n = 2+ $Pb_4Cl_2O_4$ + $Pb_{0.89}Bi_{12}O_{19.78}$ + u.p.
	$Bi_{8.66}Pb_{1.34}O_{13}[Bi_2O_2]_2Cl_6$	720	air	n = 2 + minor u.p.
	$Bi_9PbO_{13}[Bi_2O_2]_2Cl_6$	700	air	n = 2 + minor u.p.
n = 3				
$Pb_nBi_{10-n}O_{13}[Bi_2O_2]_nCl_{4+n}$	$Bi_7Pb_3O_{13}[Bi_2O_2]_3Cl_7$	720	air	n = 3 + $Bi_{12}O_{17}Cl_2$+β-Bi_2O_3+$PbBiO_2Cl$+u.p.
slight chemical deviation from formulation	$Bi_{7.5}Pb_{2.5}O_{13.25}[Bi_2O_2]_3Cl_7$	800	sealed tube	n = 3 + $PbBiO_2Cl$ + u.p.
	$Bi_{7.66}Pb_{2.34}O_{13}[Bi_2O_2]_3Cl_7$	700, 720	air	n = 3 + major u.p.
n = 4				
$Pb_nBi_{10-n}O_{13}[Bi_2O_2]_nCl_{4+n}$	$Bi_6Pb_4O_{13}[Bi_2O_2]_4Cl_8$	720	air	n = 4 + $PbBiO_2Cl$ + u.p.
slight chemical deviation from formulation	$Bi_{6.5}Pb_{3.5}O_{13.25}[Bi_2O_2]_4Cl_8$	800	sealed tube	n = 4 + $PbBiO_2Cl$
	$Bi_{6.66}Pb_{3.34}O_{13}[Bi_2O_2]_4Cl_8$	720	air	n = 4 + $PbBiO_2Cl$ + u.p.

[a]u.p. denotes unknown peaks.

Table 2. Crystal Data, Measurement, and Structural Refinement Parameters of the Studied Derivatives of $Bi_{24}O_{31}Cl_{10}$

	$Bi_{24}O_{31}Cl_{10}$[12]	$Bi_{24}O_{31}Cl_{10}$	$[Bi_8Pb_2O_{13}][Bi_2O_2]_2Cl_6$ n = 2	$[Bi_7Pb_3O_{13}][Bi_2O_2]_3Cl_7$ n = 3	$[Bi_6Pb_4O_{13}][Bi_2O_2]_4Cl_8$ n = 4	$PbBi_4O_6Cl_2$
Crystal Data						
cryst symmetry space group	monoclinic $P2/c$	monoclinic $C2/m$	monoclinic $C2/m$	monoclinic $C2/m$	monoclinic $C2/m$	tetragonal $4/mmm$
a (Å)	10.033(2)	29.486(2)	29.671(2)	29.681(2)	29.783(2)	3.9488(4)
b (Å)	7.9745(16)	3.9683(3)	3.9692(2)	3.9630(2)	3.9639(2)	
c (Å)	29.552(6)	10.0361(8)	12.2477(5)	15.1047(8)	18.3770(9)	31.038 (7)
β (deg)	88.742(4)	90.989(4)	107.492(2)	118.387(2)	125.828(2)	
V (Å^3)	2363.8(8)	1174.1(2)	1375.7(2)	1563.0(2)	1759.0(2)	483.98(13)
Z	2	2	2	2	2	2
Dx (g/cm3)	8.242	8.285	8.233	8.278	8.272	8.303
μ (mm^{-1}) (for λ Kα = 0.7107 Å)	89.601	90.191	89.819	90.358	90.335	90.355
appearance	pale green	pale green needle	pale green platelet	pale green rod	pale green needle	pale green needle
Data Collection						
λ(Mo Kα) (Å)	0.71073	0.71073	0.71073	0.71073	0.71073	0.71073
scan mode	ω and ϕ	ω and ϕ	ω and ϕ	ω and ϕ	ω and ϕ	ω and ϕ
$\theta_{(min-max)}$ (deg)	1.38 ± 28.33	1.4−26.4	1.4−30.5	1.5−25.9	1.4−28.3	2.6−26.4
R(int) (%)	0.1299	0.029	0.045	0.048	0.033	0.047
recording reciprocal space	$-13\leq h\leq 13$	$-36\leq h\leq 36$	$-42\leq h\leq 42$	$-30\leq h\leq 35$	$-36\leq h\leq 38$	$-4\leq h\leq 4$
	$-10\leq k\leq 0$	$-4\leq k\leq 4$	$-5\leq k\leq 5$	$-3\leq k\leq 4$	$-5\leq k\leq 4$	$-4\leq k\leq 4$
	$0\leq l\leq 39$	$-12\leq l\leq 12$	$-17\leq l\leq 17$	$-17\leq l\leq 18$	$-24\leq l\leq 24$	$-37\leq l\leq 38$
Refinement						
measured, indep, obsd reflns	5546	10 423, 1381, 1236	23 978, 2401, 1726	8176, 1404, 1054	15 348, 2481, 1836	849, 192, 161
no. refined params	218	77	122	102	153	16
refin method	F	F	F	F	F	F
R1(F^2)(obsd)/R1(F^2)(all)	0.063	0.0375/0.0415	0.0356/0.0524	0.0358/0.0495	0.0292/0.0430	0.059/0.0661
wR2(F^2)(obsd) /wR2(F^2)(all)	0.146	0.0361/0.0375	0.0374/0.0459	0.0459/0.0483	0.0289/0.0348	0.0610/0.0639
GOF(obsd)/GOF(all)		0.68/0.67	0.66/0.68	1.99/1.79	0.47/0.48	1.75/1.66
$\Delta\rho_{max}/\Delta\rho_{min}$ (e Å^{-3})	5.984/ −6.162	6.83/−6.14	4.70/−4.19	2.40/−2.77	3.69/ −3.26	7.08/ −3.27

ratio.[17] The series of Sillén phases[18,19] consists of α-PbO (or fluorite) $[M_2O_2]^{2+}$ layers intergrown with single $[X]$, double $[X_2]$, or triple $[M'_xX_3]$ halide layers, where X is halide atom. It produces rather simple structures found for $MBiO_2Cl$ ($X1$) (M^{2+} = Cd, Ca, Pb, etc.),[20−22] BiOCl ($X2$),[23] and $Ca_{1.25}Bi_{1.5}O_2Cl_3$ ($X3$).[24] A diversity of ordered intergrown structures have been also reported with sequences giving rise to ideal tetragonal structures with $a \sim 3.9$ Å (i.e., $\sqrt{2}/2a_{(fluorite)}$)

dx.doi.org/10.1021/ic4002708 | Inorg. Chem. 2013, 52, 8427−8435

and c varying from 6 to 50 Å dependent on the structural complexity.[20−22,24−28]

EXPERIMENTAL SECTION

All the crystals were found in polyphasic residues from the heating of the mixtures of precursors given below case by case. The starting mixtures were loaded into gold tubes, sealed, then heated at 900 °C during 10 h, and then slowly cooled (1 °C/h) down to 600 °C. The furnace was then switched off, and crystals were handly selected. In the cases where fluxes were used, washing with hot water was required to separate crystals from the flux. The following reagents with their respective purities have been used in the syntheses: Bi_2O_3 (Aldrich 99.9%), BiOCl (Alfa Aesar, ultrapure), $PbCl_2$ (Alfa Aesar, 99.9%), PbO (Aldrich, 99.9%). Table 1 gives a summary of our attempts to prepare polycrystalline compounds of the several phases concerned in this work according to the $[Pb_nBi_{10-n}O_{13}][Bi_2O_2]_nCl_{4+n}$ formulation or using slight deviations of the Bi/Pb ratio in various experimental conditions.

$Bi_{24}O_{31}Cl_{10}$ (Arppe's Compound). The crystals of were found in the polycrystalline residue from the melt of 10 (wt %) of the (4BiOCl +3$KMnO_4$) mixture in 90 (wt %) of KCl which was taken as a flux. Note that in the recent literature crystals of this compound were grown from a mixture of $BiCl_3$ and Bi_2O_3 in 1:3.1 ratio at 450 °C K in a sealed quartz ampule.[12]

$[Pb_2Bi_8O_{13}][Bi_2O_2]_2Cl_6$ (n = 2 Term). The crystals were found in the melt of the mixture $3Bi_2O_3$ + 6BiOCl + PbO + CuO. The powder was obtained as a single polycrystalline phase from the stoichiometric mixture of $PbCl_2$, Bi_2O_3, and BiOCl heated with several intermediate grindings at 750 °C in an evacuated quartz ampule. It was identified by comparison to the theoretical XRD pattern calculated from the refined crystal structure, Table 1. The lattice parameters refined from the powder diffraction are a = 29.6643(8) Å, b = 3.9694(2) Å, c = 12.2489(4) Å, β = 107.39(2)° which confirms the preparation of the n = 2 term.

$[Bi_7Pb_3O_{13}][Bi_2O_2]_3Cl_7$ (n = 3 Term) and $[Bi_6Pb_4O_{13}][Bi_2O_2]_4Cl_8$ (n = 4 Term). The crystals were obtained from the same melt of composition 2PbCl + 5BiOCl + $5Bi_2O_3$. The attempts to reproduce them in powder as a pure phase were unsuccessful. However, the peaks of the theoretical patterns, calculated from the respective single crystal XRD data, were found systematically in preparations which validate the possibility to prepare the phases, Table 1.

$PbBi_4O_6Cl_2$. The crystals were found in the molten residue of 5 (wt %) of the (2PbO + $3Bi_2O_3$ + $6MnO_2$) mixture in the flux of ($6Bi_2O_3$ + 6BiOCl) 95 (wt %). The corresponding powder was obtained as a single polycrystalline phase from the stoichiometric mixture of $PbCl_2$ and Bi_2O_3 heated at 750 °C in an alumina crucible, after several intermediate grindings. It was obtained as a single phase, see Table 1. The lattice parameters refined from the powder diffraction pattern lead to a = 3.9539(8) Å and c = 31.072(2) Å in good adequation with the lattice parameters refined from the single crystal data (see below).

Characterization. The single crystal XRD data of all the investigated samples have been collected using a Bruker Apex Duo diffractometer with a Mo−IμS microfocus tube (λ = 0.710 73 Å). The intensity data have been extracted from the collected frames using the program SAINT-Plus 6.02.[29] The lattice parameters have been defined from the complete data set. Absorption corrections have been performed using multiscan methods using SADABS.[30] The data collection and pertinent data of the refinements for all single crystals studied in this work are gathered in the Table 2.

Author: If your meaning has not been retained anywhere in Table 2, please clarify in galley corrections.

X-ray powder diffraction analysis of all the powder samples have been performed at room temperature in the angular 2Θ range of 5−80° with the scan step width of 0.02° using the D8 Advance Bruker AXS diffractometer. Pattern matching was performed on Fullprof software.[31]

Electrical measurements were performed on $[Pb_2Bi_8O_{13}]$-$[Bi_2O_2]_2Cl_6$ (n = 2 term) by impedance spectroscopy between room temperature and 655 °C using a Solartron 1260 impedance analyzer with a 500 mV amplitude signal over the 0.1 Hz to 10 MHz frequency range. Gold electrodes were deposited by evaporation at both sides of a sintered pellet (~80% dense). Three heating/cooling cycles were applied to the sample, while only the third one is presented below, for which extra-densification effects are negligible. All impedance diagrams were normalized using the thickness/surface geometrical factor. Fitting of impedance spectra was performed using local software to extract characteristic of typical RC circles.

Photoluminescence excitation and emission spectra were collected on a FluoroMax HORIBA fluorescence spectrometer within the spectral range 250−800 nm using excitation and emission slit widths of 2 nm at 10 K. Each excitation spectrum was taken while observing emission at the predetermined emission wavelength maxima, and likewise, the emission spectra was taken while exciting at the sample's excitation wavelength maxima.

RESULTS AND DISCUSSION

The structure of Arppe's compound, $Bi_{24}O_{31}Cl_{10}$, was first refined in 1942 (space group $A2/m$, a = 9.99 Å, b = 3.97 Å, c = 29.44 Å, β = 88.7°) and revised one decade ago in the a, 2b, c supercell (space group $P2/c$),[11,12] see Table 2. Its crystal structure projected along the b-axis is shown in Figure 1a. It is

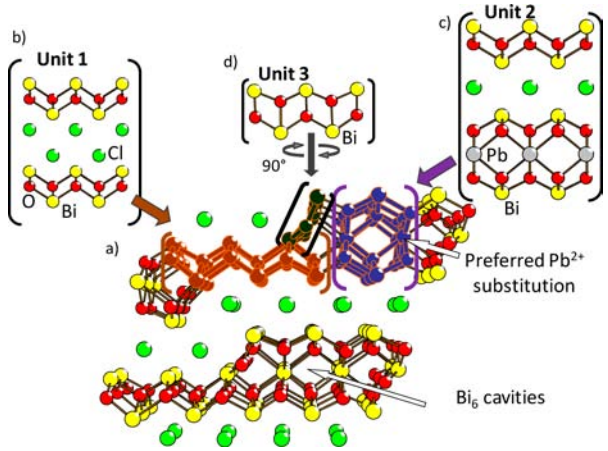

Figure 1. (a) Structure of Arppe's compound as an assembly of building units: (b) unit 1, (c) unit 2, (d) unit 3.

formed of crenel-like infinite $[Bi_{24}O_{30}]^{10+}$ layers separated by single $[Cl_{10}]^{10-}$ layers. From the viewpoint of modular chemistry it is convenient to identify and formulate elementary units for the description/design of new compounds. In this frame, the $[Bi_{24}O_{30}]^{10+}$ layers can be sliced into three building units.

For unit 1, the Bi/O modules which are formed of a linear portion of a fluorite like $[Bi_2O_2]^{2+}$ layer, see Figure 1b. Similar layers are well-known and found for instance in the BiOCl crystal structure denoted (X2) due to the double-thickness of the chloride layers,[23] see Figure 2a.

For unit 2, thicker modules play the role of "stairs", in the 2D-crenel topology of $[Bi_{24}O_{30}]^{10+}$ layers, Figure 1c. They mainly correspond to portions of "3-cations thick" fluorite layers portions similar to $[BaBi_2O_4]^0$ found $BaBi_4O_6Cl_2$[32] with Bi^{3+} replacing the central Ba^{2+} cations. In this Article, we will describe the new compound $PbBi_4O_6Cl_2$ with Pb^{2+} in these central sites, Figure 2b. As detailed below, in Arppe's compound $Bi_{24}O_{31}Cl_{10}$, central cavities created by Bi_6 octahedra are partially occupied by extra oxygen atoms (O_{octa}). Our reinvestigation of the Arppe's crystal structure agrees well with that point, but as it is shown later the incorporation of Pb^{2+} into

dx.doi.org/10.1021/ic4002708 | Inorg. Chem. 2013, 52, 8427−8435

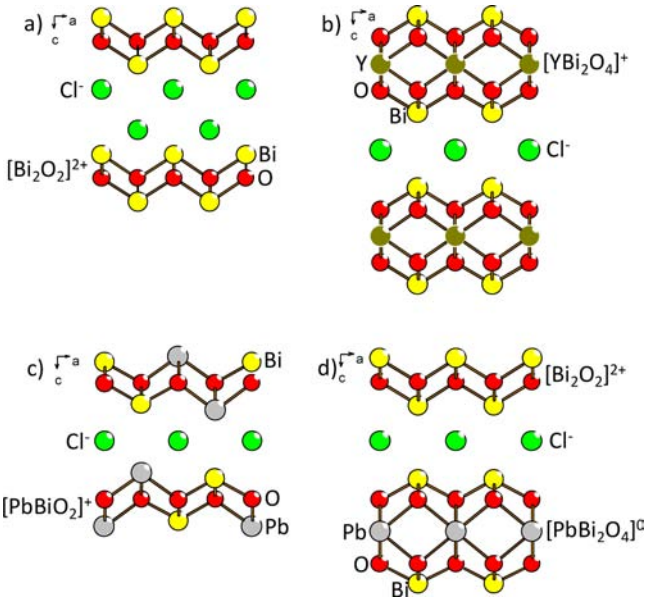

Figure 2. Comparison of layered modules in the crystal structures of (a) BiOCl, (b) Bi_2LnO_4Cl, (c) $PbBiO_2Cl$, and (d) $PbBi_4O_6Cl_2$ (this work).

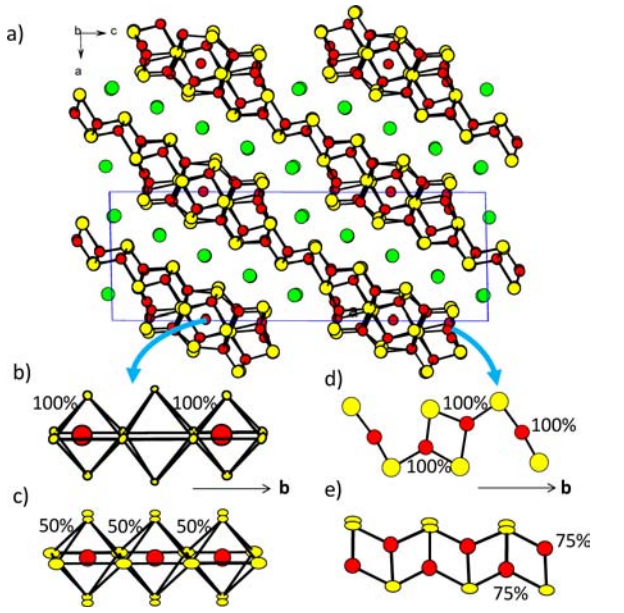

Figure 3. (a) Crystal structure of Arppe's compound. Occupancy of oxygen atoms in the Bi_6 cavities: (b) according to ref 12, (c) according to our refinement in the subcell. Ordered O/Bi arrangement in the bordering units 3: (d) from ref 12, (e) according to our refinement in the subcell.

these units systematically removes this interstitial anion. The condensation between unit 1 and unit 2 is performed by edge sharing of OBi_4 tetrahedra and involves a third unit (unit 3) bordering the junction.

For unit 3, the outer side of the "stair" is formed by a chain of partially filled anion-centered $(O,\square)Bi_3$ triangles, Figure 1d. These kind of bordering OBi_3-based units are often found in compounds made of finite or infinite topologies of OBi_4 triangles with square angles corners such as columns, open tunnels, crenel-planes.[19,33] For instance, the structure of $Bi_9A_2ClO_{18}$ (A = P, As) was recently redescribed using similar subunits.[34]

Concerning Arppe's compound, in the most recent model refined by Eggenweiler et al.[12] two main crystallographic features are responsible for the *b*-axis doubling, see Figure 3a. First, the ordering of the oxygen atoms (O_{octa}) in half of the Bi_6 cavities of the stair-like junctions (units 2), Figure 3b. Second, the fully ordered O/Bi arrangement at the bordering sites of the thick junctions (units 3), giving a sequence of OBi_2 and OBi_3 units ordered along the *b*-axis, see Figure 3d. However, our analysis of reprepared single crystals shows a slightly different disordered topology. We also found evidence of the *b*-doubling, but with rather weak and broad supercell spots. Our attempts to consider the reported supercell model yielded high *R* values: $R = 0.18$, $wR = 0.25$. On the opposite, the consideration of the original subcell-only reflexions ($a = 29.486(2)$ Å, $b = 3.9683(3)$ Å, $c = 10.0361(8)$ Å, $\beta = 90.989(4)°$, space group $C2/m$, $R = 0.0375$, $wR = 0.0361$) leads to the disordered features shown in Figure 3c–e. The oxygen occupancies were constrained to obtain the same stoichiometry as the fully ordered model which involves 50% occupancy of O_{octa} (=O9), and 75% occupancy of two oxygen atoms of unit 3, (Supporting Information Table S1). A similar oxygen distribution will be used for all new compounds related to the Arppe's compound, to be further presented (Tables S1–S15). The expansion or not of the crystal structure in a doubled *b* supercell most probably pictures an ideal ordering reached in particular equilibrium conditions while our standard thermal conditions likely generate local ordered domains only. We note that Eggenweiler et al. did not succeed in refining a supercell model for the isostructural oxobromide $Bi_{24}O_{31}Br_{10}$.[12]

Bi^{3+}/Pb^{2+} Ordering in the New $PbBi_4O_6Cl_2$. Taking into account the need for identification of different modules that assemble in the series of new compound described above, the new $PbBi_4O_6Cl_2$ appears as a parent term. It crystallizes in the $I4/mmm$ space group ($a = 3.9488(4)$ Å, $c = 31.038(7)$ Å) with a layered structure which corresponds to the stacking sequence $[Bi_2O_2]^{2+}[Cl]^-[PbBi_2O_4]^0[Cl]^-$ (Figure 2d). $[Cl^-]$ layers are simple, in constrast to their double thickness in BiOCl, Figure 2a. It corresponds to an intergrowth between the Bi_2LnO_4Cl[35] (Figure 2b) and the $MBiO_2Cl$ (X1) (Figure 2c) structures, but with Pb^{2+} instead Ln^{3+} and Bi^{3+} instead M^{2+} in the two distinct metal layers, respectively. The compound is isostructural with $BaBi_4O_6Cl_2$ where neutral $[BaBi_2O_4]^0$ layers also exist.[32] $PbBi_4O_6Cl_2$ is to our knowledge the first example of Pb^{2+} in the central sites of such layers generally hosting large cations without lone pair electrons (Ba^{2+}, Ln^{3+}). It follows that, in $PbBi_4O_6Cl_2$, the lone pair is not active and Pb^{2+} is at the center of a regular PbO_8 quadratic prism (Pb–O bonds: $8 \times 2.52(3)$ Å). The Bi/Pb segregation into distinct sites is complete, and Bi^{3+} occupies a typical BiO_4Cl_4 tetragonal antiprism (Bi–O, $4 \times 2.23(2)$ Å; Bi–Cl, $4 \times 3.437(9)$ Å). One should note that in $[PbBiO_2]$ layers of the $PbBiO_2Cl$-X1 structure the Pb/Bi ordering is also complete (Bi–O, 4×2.27 Å vs Pb–O, 4×2.44 Å and Bi–Cl, 4×3.42 Å vs Pb–Cl, 4×3.26 Å), but both cations are located in the same layers and both have a stereoactive lone pair, Figure 2c. Typically, this disparity in terms of M–O and M–Cl distances can be regarded as a precious tool to distinguish Bi and Pb in complex mixed Bi/Pb compounds as follows. Bond valence calculations using the sums of M–O and M–Cl contributions using bond valence parameters of M–Cl bonds from Brese and O'Keeffe[36] and more recent ones of M–O bonds revisited by S. Krivovichev[37]

dx.doi.org/10.1021/ic4002708 | *Inorg. Chem.* 2013, 52, 8427–8435

lead to BVS values that are almost correct: BVS_{Bi1} = 2.67, BVS_{Bi2} = 2.97, BVS_{Pb1} = 2 .25 (Table 3).

Table 3. BVS of the Sites Most Likely for Pb^{2+} Occupancy: Bi6 in Arppe's Compound, Pb7 in n = 2; Pb8 in n = 3; Pb8 in n = 4; Bi1, Bi2, and Pb1 in $PbBi_4O_6Cl_2$

atom 1	atom 2	D	v_{Bi}[a]	v_{Pb}[a]
Arppe's Compound				
Bi6	1 × O5	2.317(18)	0.51	0.48
	2 × O3	2.431(10)	0.80	0.76
	1 × O1	2.606(16)	0.28	0.27
	1 × O5	2.613(19)	0.27	0.26
	2 × O6	2.619(12)	0.54	0.52
	1 × O7	2.736(39)	0.21	0.21
	2 × O9	2.7838(8)	0.38	0.37
		BVS (2 × O9)	2.99	2.88
		BVS (abs O9)	2.61	2.51
n = 2				
Pb7	1 × O6	2.297(18)	0.53	0.50
	2 × O7	2.432(8)	0.80	0.76
	1 × O2	2.584(15)	0.29	0.28
	1 × O6	2.602(19)	0.28	0.27
	2 × O5	2.631(9)	0.53	0.51
	1 × O8	2.807(35)	0.18	0.18
		BVS	2.60	2.50
n = 3				
Pb8	1 × O8	2.268(25)	0.56	0.53
	2 × O6	2.427(11)	0.80	0.77
	1 × O8	2.559(27)	0.31	0.29
	1 × O3	2.564(26)	0.30	0.29
	2 × O7	2.626(12)	0.53	0.51
	1 × O9	2.774(55)	0.20	0.19
		BVS	2.70	2.59
n = 4				
Pb8	1 × O8	2.304(22)	0.52	0.50
	2 × O7	2.421(7)	0.81	0.78
	1 × O4	2.564(19)	0.30	0.29
	1 × O8	2.579(23)	0.29	0.28
	2 × O9	2.619(8)	0.54	0.52
	1 × O10	2.769(38)	0.20	0.19
		BVS	2.67	2.56
$PbBi_4O_6Cl$				
Bi1	4 × O1	2.323(2)	2.00	1.91
	4 × Cl1	3.337(11)	0.67	0.45
		BVS	2.67	2.36
Bi2	4 × O2	2.231(24)	2.42	2.30
	4 × Cl1	3.437(11)	0.54	0.34
		BVS	2.97	2.65
Pb1	8 × O2	2.584(29)	2.32	2.24
		BVS	2.32	2.24

[a] (R, b) parameters being for Pb^{2+}–O (1.963, 0.49) and Bi^{3+}–O (1.990, 0.48).[37]

$[Pb_nBi_{10-n}O_{13}][Bi_2O_2]_nCl_{4+n}$ Compounds (n = 1–4). If one considers the condensation of the unit 1 and units (2 + 3) as shown in Figure 4, a generic formulation $[Bi_{10-n}Pb_nO_{13}]^{unit2+3}[Bi_2O_2]_n^{unit1}Cl_{4+n}$ can be given to the compounds formed by progressive elongation of the linear unit 1 by addition of extra OBi_4 tetrahedra and by partial substitution of Bi^{3+} for Pb^{2+} in unit 2 in order to reach electroneutrality. Here the central oxygen O_{octa} of unit 2 of the parent Arppe's compound was not considered for the formulation since it was never observed either in the single crystals of the novel mixed Bi/Pb n = 2, 3, 4 members or in the similar cavities offered by the crystal structure of $PbBi_4O_6Cl_2$ with similar but infinite $[BiPbO_4]$ layers. The role of O_{octa} in $Bi_{24}O_{31}Cl_{10}$ is most probably to compensate for excess positive charge created by adjacent Bi^{3+}, and the absence of the former in the Pb-containing compounds is an indicator for the preferred location of Pb^{2+} in unit 2. When an extra need for Pb^{2+} cations is required to keep electroneutrality, we have set them in the cationic sites of unit 3 shown in Figure 1a. This aspect will be discussed later concerning the veracity of the Pb/Bi crystallographic discrimination that we applied to further compounds.

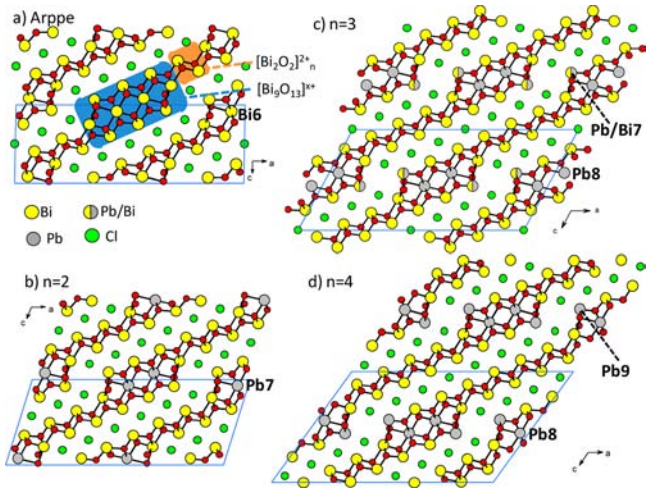

Figure 4. Structures of the $[Pb_nBi_{10-n}O_{13}][Bi_2O_2]_nCl_{4+n}$ members: (a) hypothetical $[PbBi_9O_{13}][Bi_2O_2]Cl_5$, n = 1, (b) $[Pb_2Bi_8O_{13}]$-$[Bi_2O_2]_2Cl_6$, n = 2, (c) $[Pb_3Bi_7O_{13}][Bi_2O_2]_3Cl_7$, n = 3, and (d) $[Pb_4Bi_6O_{13}][Bi_2O_2]_4Cl_8$, n = 4.

Hypothetical n = 1 Term $[PbBi_9O_{13}][Bi_2O_2]Cl_5$. It would correspond to a slightly modified crystal structure of Arppe's compound $Bi_{24}O_{31}Cl_{10}$ after doping with Pb^{2+} for removal of O_{octa} for reasons explained above. Here we consider that the Pb^{2+} substitution is efficient in the unit 3 only, preferentially in the sites shown in gray in Figure 4a. As briefly described above, we failed to prepare the single polycrystalline phase from the stoichiometric mixture of $PbCl_2$, Bi_2O_3, and BiOCl heated at 750 °C in an alumina crucible or evacuated quartz ampule, after several intermediate grindings. However, in some cases, the presence of an isostructural compound, i.e., $Bi_{24}O_{31}Cl_{10}$, was confirmed in the powder XRD pattern, but the presence of other phases prevents us from concluding about the real incorporation of mixed Bi^{3+}/Pb^{2+} cations in the structure which would yield the real n = 1 compound. Also, in one of our tests the prepared compound mainly corresponded to the n = 2 term described below, accompanied by a weak amount of a second unidentified phase. It seems that the incorporation of lead favors the preparation of this phase which appears to be the most stable of the n = 1 to n = 4 series. However, the formulation of the n = 1 term, even if hypothetical, remains necessary to pave the way from the original Arppe's compound until the further n = 2, 3, and 4 compounds.

***n* = 2 Term $[Pb_2Bi_8O_{13}][Bi_2O_2]_2Cl_6$.** The full series of compounds n = 1–4 is shown in Figure 4. For n = 2, the crystal structure refinement leads to R = 0.0356, wR = 0.0374, space group $C2/m$, with lattice parameters a = 29.671(2) Å, b = 3.9692(2) Å, c = 12.2477(5) Å, β = 107.492(2)°. Precession

dx.doi.org/10.1021/ic4002708 | Inorg. Chem. 2013, 52, 8427–8435

images show no sign for the *b*-doubling. It corresponds to the formula $[Pb_2Bi_8O_{13}][Bi_2O_2]_2Cl_6$. No oxygen was located in the O_{octa} sites of unit 2, which leads us to consider Pb^{2+} cations in the central sites of these units (=Pb7 site) as shown in gray in Figure 4b. Once more, this choice was done by analogy to the structure of $PbBi_4O_6Cl_2$. In addition, the average Bi−O distance concerning the BiO_4 pyramids of unit 1 is 2.26 Å which is likely for bismuth cations by analogy with the $PbBi_4O_6Cl_2$ and Arppe's compound. The occupancies of oxygen of unit 3 have been fixed to 75% similarly to our refinement of the disordered Arppe's compound in absence of *b*-doubling. It is noteworthy that two bismuth positions have been split on satellite positions (Bi4a/Bi4b and Bi6a/Bi6b) in order to minimize local residual electronic density peaks observed on Fourier-difference maps. This could create a picture of a local Pb/Bi mixed occupancy, but we preferred for the full series a unified model with Pb^{2+} cations located solely in the units 2 + 3. We already announced in Table 1 the successful preparation of the corresponding powder using the stoichiometric ratio between all elements. The pattern matching is shown in Figure 5 (a = 29.6643(8) Å, b = 3.9694(2) Å, c = 12.2489(4) Å, β = 107.39(2)°, and V = 1376.35(7) Å^3 with χ^2 = 1.65).

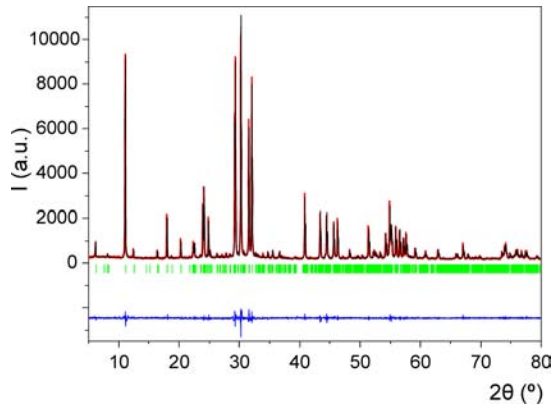

Figure 5. XRD profile fitting of the compound $[Pb_2Bi_8O_{13}]$-$[Bi_2O_2]_2Cl_6$, n = 2, with refined parameters a = 29.6643(8) Å, b = 3.9694(2) Å, c = 12.2489(4) Å, β = 107.39(2)°.

***n* = 3 Term $[Pb_3Bi_7O_{13}][Bi_2O_2]_3Cl_7$.** The projection of the crystal structure is shown in Figure 4c. The crystal structure was refined in the space group $C2/m$ leading to R = 0.0358, Rw = 0.0459, lattice parameters a = 29.681(2) Å, b = 3.9630(2) Å, c = 15.1047(8) Å, β = 118.387(2)°. Here, Pb^{2+} cations have been set in the central sites of unit 2 (100% Pb8) and in the bordering cationic sites common to units 2 and 3 (50% Bi7−50% Pb7) as shown in Figure 4c. The oxygen atoms of unit 3 are 75% occupied. No cationic atom was found split during the refinement process. Also, as for the previous case, no residual electron density was located in the O_{octa} sites which are anion-empty. Once more the presence of Bi^{3+} species only in unit 1 is supported by the concerned Bi−O distances: the three independent Bi atoms involved in these units have similar BiO_4 coordination with an average Bi−O distance of 2.26−2.27 Å reminiscent of the bismuth−oxygen coordination in $PbBi_4O_6Cl_2$ and Arppe's compound. This phase was prepared in a polycrystalline state but with some secondary phases such as $Bi_{12}O_{17}Cl_2$, β-Bi_2O_3, or $PbBiO_2Cl$, see Table 1.

***n* = 4 Term $[Pb_4Bi_6O_{13}][Bi_2O_2]_4Cl_8$.** The structure of the last term of the series solved in $C2/m$ space group as well in the unit cell parameters is described in the following: a = 29.783(2) Å, b = 3.9639(2) Å, c = 18.3770(9) Å, β = 125.828(2)°, with the refinement parameters R = 0.0292, Rw = 0.0289. In this case, Pb^{2+} cations have been set in the central sites of unit 2 (100%) as well as in the bordering cationic sites common to units 2 and 3 (100% Pb8 and Pb9) as shown in Figure 4d. We note that site Pb9 was split into satellite positions Pb9a (66%) and Pb9b (44%) to lower residual electron density. Once again, the occupancies of the oxygen atoms of unit 3 were fixed to 75%. As in the previous n = 3 case, no pure polycrystalline sample was obtained for this term, even if the major presence of the compounds was observed in some cases, see Table 1.

As detailed for each compound, the choice for preferential location of Pb^{2+} cations is supported by the Bi−O distances found close to 2.27 Å in unit 1 which are similar to Bi−O distances in $PbBi_4O_6Cl_2$ and $Bi_{24}O_{31}Cl_{10}$ while Pb−O distances in similar PbO_4 coordinations are closer to 2.44 Å. Therefore, we propose that the cationic sites of unit 1 are filled by 100% Bi. In addition the strict localization of all Pb^{2+} particular subunits enables the setting of the general formula $_{unit2+3}[Bi_{10-n}Pb_nO_{13}]_{unit1}[Bi_2O_2]_nCl_{4+n}$ that describes the full series from the hypothetical n = 1 term (modified Arppe's compound), which is not clearly confirmed on powder, to the refined n = 2, 3, and 4 compounds. From the distances listed in the Supporting Information it is clear that, inside unit 2, the mean Pb/Bi−O distances seem to increase on increasing n which supports the introduction of largest Pb^{2+} in these units. Particularly, in these units taking into account our proposition for Pb/Bi ordering in distinct sites, the Pb−O distances are close to 2.3 Å while Bi−O distances are closest to 2.2 Å. However, several features seem to indicate that this ordering is most probably idealized and that the reality is more contrasted: (i) The split of some atoms in unit 1 (for instance Bi4a/Bi4b in the n = 2 term) could suggest the presence of mixed Bi/Pb sites in these structural fragments. (ii) The bond valence sum calculations on the position preferred for Pb^{2+} (i.e., Bi6 in Arppe's compound, Pb7 for n = 2, Pb8 for n = 3, Pb8 for n = 4) are given in Table 3. For our refinement of the crystal structure of Arppe's compound with 50% of O_{octa} in the interstices of unit 2, bond valence sum was calculated in absence or presence of O_{octa} (=O9) in the Bi and Pb hypotheses. Clearly, the presence of O9 stabilizes the presence of Bi^{3+} in this site (S_{Bi3+} with O9 = 2.99 against S_{Bi3+} without O9 = 2.61). In the n = 2, 3, and 4, where the presence of O_{octa} sites was never observed, the calculations show an underbonded character in the Bi^{3+} hypothesis (S_{Bi3+} = 2.5−2.7) and an overbonded character in the Pb^{2+} hypothesis (S_{Pb2+} = 2.5−2.6) which would play in favor of a mixed distribution rather than the preferential filling of this site by Pb^{2+} only. On the other hand, bond valence sums remain an empirical value which should not be considered *stricto sensu*. At least, the preferred occupancy of this position by Pb^{2+} is reminiscent of the $[PbBi_2O_4]$ blocks in $PbBi_4O_6Cl_2$, and can be proposed as an ideal scheme, but even in this ordered compound, BVS calculations for Bi1, Bi2, and Pb1 sites also lead to intermediate values, i.e., +2.67 (Bi1), +2.97 (Bi2), and +2.24 (Pb1) in absence of mixed sites.

Electric Properties. According to the partial disorder that was refined over both cationic and anionic positions for all the compounds of the $[Pb_nBi_{10-n}O_{13}][Bi_2O_2]_nCl_{4+n}$ series, it sounds interesting to evaluate the potential for anionic conductivity in such structures. In addition, the existence of chloride planes similar to those found in Cl^- conduction rare earth oxychlorides may also favor halide conductivity. The n = 2 term

dx.doi.org/10.1021/ic4002708 | *Inorg. Chem.* 2013, 52, 8427−8435

was selected as the only compound prepared as a polycrystalline single phase in our study. The conditions of measurements of our impedance spectra were briefly given in the Experimental Section. Typical semicircles are appearing above 250 °C and are better shaped on increasing temperature. For instance at 655 °C (see inset of Figure 6), we observe two circles between 0.1

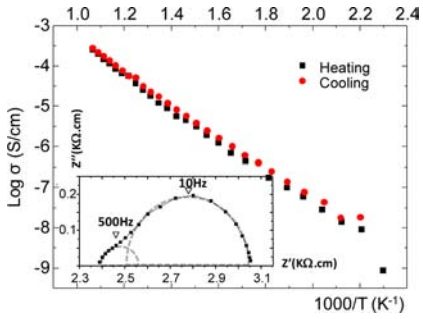

Figure 6. Arrhenius plot of the conductivity of the n = 2 term $[Pb_2Bi_8O_{13}][Bi_2O_2]_2Cl_6$. Inset: Nyquist plot for the measurement at 665 °C with indication of the relaxation frequencies for each events.

Hz and 10 kHz while high frequency points are out of the (Z', Z'') Nyquist diagrams. The intersection of the highest frequency circle with the Z' axis is 2.4 kΩ cm which indicates a significant resistive contribution in the equivalent electric circuit. Together with the two overlapped circles it would correspond to a pure resistance in series with two RC elements. This shape of impedance diagram is typical for conventional polycrystalline ionic conductors; the high frequency bulk semicircle describes the electrical properties of the grains of the ceramics, and the low frequency additional contribution is due to the blocking effects of charge carriers at grain boundaries. However, the relaxation frequency (f_{max}) of the low frequency diagram is very low (~10 Hz) and coincides better with process associated with the oxygen adsorption–desorption on the gold electrode and surface diffusion of anionic oxygen species.[38] Then, this semicircle was assigned to both blocking effects and electrode reaction. It follows that the Arrhenius behavior shown in Figure 6 was plotted considering the resistive offset and the RC circuit assigned to the bulk effect (with a rather low relaxation frequency ~500 Hz at 655 °C). It shows a good reproducibility between data taken on heating and cooling, and the calculated activation energy from the Arrhenius law is 0.78 eV. For the purpose of identifying the mobile anions (Cl^- vs O^{2-} vs mixed of both) species, changing O_2 or Cl_2 gas pressure should be further performed, but it is out of the scope of our Article. Despite the well-ordered Cl^- sublattice, at this stage one could imagine a contribution of Cl^- conductivity, since the order of magnitude of the conductivity is comparable to what was observed in Ca-doped LaOCl,[39] taking into account the low frequency associated with the bulk semicircle compatible with less mobile Cl^- anions.

Luminescence Properties. Cations with ns^2 electronic configuration, like Bi^{3+}, Pb^{2+}, Tl^+, and Sb^{3+}, are very promising candidates for applications because they are able to exhibit efficient excitation and extremely bright emission due to parity allowed, fast $s^2 \leftrightarrow sp$ electronic transitions. Spectroscopic properties of Bi^{3+} and Pb^{2+} have been extensively investigated because these ions are effective activators for luminescent materials widely used in scintillation detectors, lamps, or X-ray phosphors.[40−44]

The ground state of the $6s^2$ configuration is $^1S_0$ while the 6s6p excited states give rise to triplet ($^3P_0$, $^3P_1$, and $^3P_2$) and the $^1P_1$ singlet levels. Transitions between the ground state $^1S_0$ and $^3P_0$, $^3P_1$, $^3P_2$ are spin forbidden; however, the $^1S_0 \rightarrow {}^3P_1$ transition (A-band) becomes partly allowed due to coupling of $^3P_1$ and $^1P_1$ states. The $^1S_0 \rightarrow {}^1P_1$ (C-band) is an allowed electric dipole transition.

In the case of Bi^{3+} ions, emission originated by the $^3P_1 \rightarrow {}^1S_0$ transition is usually detected at room temperature, but at low temperature the highly forbidden $^3P_0 \rightarrow {}^1S_0$ emission is also observed.[45] For Pb^{2+} the situation is slightly different. Commonly, the luminescence is described by $^1S_0 \rightarrow {}^3P_{1,2}$ + $^1P_1$ transitions for excitation and $^3P_1 \rightarrow {}^1S_0$ for emission. Another optical transition (D-band) can appear in both cases, which is probably due to an electronic charge transfer between the metal and the ligand or between two metals.[46] It occurs mostly if there is a significant coupling between the $^3P_1$ and $^3P_0$ states and the electronic states of nd^{10}/nd^0 ions (for example, V^{5+} or Ga^{3+}).[47] These transitions are quite diverse and depend strongly on the environment conditions of Bi^{3+}/Pb^{2+} in a host and also on their crystallographic site.

In this Article, we report preliminary results of the photoluminescence of $PbBi_4O_6Cl_2$, $[Pb_2Bi_8O_{13}][Bi_2O_2]_2Cl_6$, as well as $BaBi_4O_6Cl_2$; details, like temperature dependent measurements, quantum yields, and lifetimes, will be published elsewhere. All compounds show a strong red emission at low temperatures if irradiated with a UV lamp, which is very unusual for s^2 ions and, thus, extremely remarkable. The respective spectra are depicted in Figures 7 and 8, while the data are collected in Table 4. The emission is, unfortunately, quenched in all cases at room temperature, which prevents the utilization for applications.

For $PbBi_4O_6Cl_2$ the emission band is located at 14 450 cm^{-1}, while the excitation band starts at about 19 000 cm^{-1} with a maximum at 22 420 cm^{-1} (Figure 7, Table 4). The Stokes shift can therefore be determined to 7970 cm^{-1}. $[Pb_2Bi_8O_{13}]$-$[Bi_2O_2]_2Cl_6$ shows an emission band with a maximum at 14 286

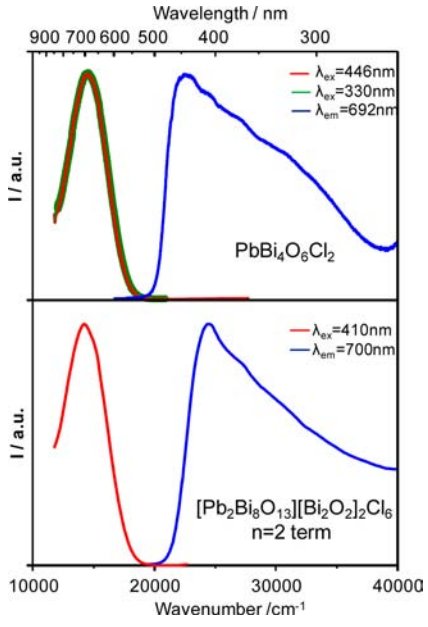

Figure 7. Fluorescent spectra of $PbBi_4O_6Cl_2$ and $[Pb_2Bi_8O_{13}]$-$[Bi_2O_2]_2Cl_6$ (n = 2 term) at 10 K.

dx.doi.org/10.1021/ic4002708 | Inorg. Chem. 2013, 52, 8427−8435

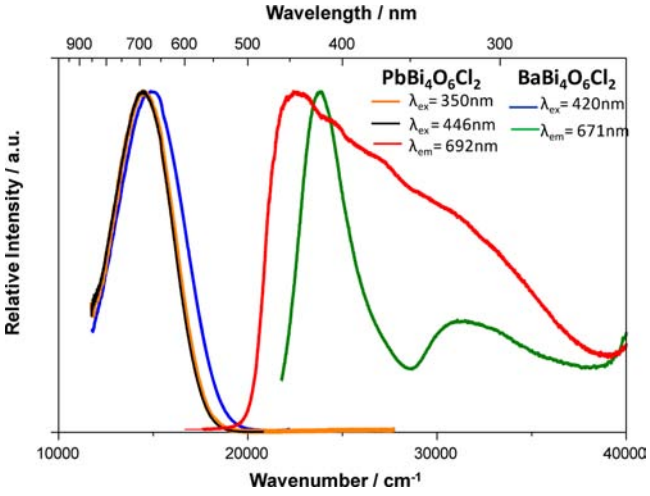

Figure 8. Comparison between fluorescent spectra of $PbBi_4O_6Cl_2$ and $BaBi_4O_6Cl_2$ at 10 K.

Table 4. Optical Properties of $PbBi_4O_6Cl_2$, n = 2 Term $[Pb_2Bi_8O_{13}][Bi_2O_2]_2Cl_6$ and $BaBi_4O_6Cl_2$: Excitation and Emission Maximum and Stokes Shift

	$PbBi_4O_6Cl_2$	n = 2	$BaBi_4O_6Cl_2$
excitation/cm^{-1} (maximum)	22 420	24 390	23 810
emission/cm^{-1} (maximum)	14 450 (red)	14 286 (red)	14 903 (red)
Stokes shift/cm^{-1}	7970	10 104	8907

cm^{-1}; the excitation band has an onset at about 20500 cm^{-1} and a maximum at 24390 cm^{-1}. The Stokes shift is 10104 cm^{-1}.

Both $PbBi_4O_6Cl_2$ and $[Pb_2Bi_8O_{13}][Bi_2O_2]_2Cl_6$ possess two s^2 cations (Bi^{3+} and Pb^{2+}). The energetic position of the excited states and, thus, the location of the emission and excitation bands are in general at similar energies.[48] Therefore, it is impossible to assign excitation and more particularly emission bands to transition of the respective ions. Due to this reason we synthesized and investigated the luminescence properties of $BaBi_4O_6Cl_2$, which is isotypic to $PbBi_4O_6Cl_2$, with very comparable cell parameters, and has, thus, the same Bi and Ba/Pb crystallographic site.[35] The shape and the position (λ_{max} = 14 903 cm^{-1}) of the emission band of $PbBi_4O_6Cl_2$ are very similar to those of $BaBi_4O_6Cl_2$ (Figure 8), and both can therefore most probably be assigned to the $^3P_0 \rightarrow {}^1S_0$ transition of Bi ions. In contrast, the excitation bands of $PbBi_4O_6Cl_2$ and $BaBi_4O_6Cl_2$ are quite different. For $BaBi_4O_6Cl_2$ two excitation bands located at 23 810 and 31 000 cm^{-1} could be detected, which can be assigned to $^1S_0 \rightarrow {}^3P_1$ and $^1S_0 \rightarrow {}^3P_2$ transitions of the Bi^{3+} ion. The high energy transition becomes in general allowed at low temperatures but with small intensity. The excitation spectrum of $PbBi_4O_6Cl_2$ contains some additional transitions (Figure 8), which can be assumed to be originated by Pb^{2+} transitions. Because the emission spectrum of $PbBi_4O_6Cl_2$ shows exclusively Bi emission, a complete Pb−Bi energy transfer after Pb excitation can be assumed (Figure 9), although some additional investigations, like lifetime measurements, are necessary to overlay this statement. The same behavior can be supposed for $[Pb_2Bi_8O_{13}][Bi_2O_2]_2Cl_6$, where the shift of the maxima of the excitation and emission bands relative to $PbBi_4O_6Cl_2$ can be explained by the different structures of both compounds.

As we stated above, the red emission of the compounds presented here is quite unique. Parke and Webb noticed red

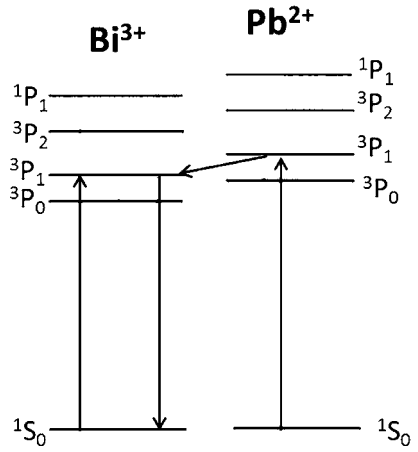

Figure 9. Sketch of charge transfer between Pb^{2+} and Bi^{3+}.

emission from Bi^{3+} in calcium phosphor glasses,[49] but after recent reinvestigation, Qiu et al.[50] concluded that this emission is originated by Bi^{2+}. More recently, Qiu et al. found a surprising near-to-mid-IR luminescence in $Bi_5(AlCl_4)_3$, which was attribute to Bi_5^{3+} clusters.[51] $Bi_{12}GeO_{20}$ is also reported to show an emission band in the red region at low temperature, but also an additional band at higher energy was detected.[48] To the best of our knowledge the compounds reported here are the first examples for red emission of Bi^{3+} doped in an oxychloride host. In general, red emission in Bi-doped compounds is usually assigned to Bi^{2+}.[52,53]

CONCLUSION

We propose here the description of a novel homologous series of general formula $[Pb_nBi_{10-n}O_{13}][Bi_2O_2]_nCl_{4+n}$ by the assembly of different kinds of well-separated units stacked in the new layered $PbBi_4O_6Cl_2$. The similarities of the new series with the parent well-known Arppe's compound is unique and lead to an extended family with sizable crenel [Bi/Pb/O] walls isolated by chloride ions. We recall that historically Arppe's compound was famous until Sillén and Edstrand spent a long time to solve its complex crystal structure which was finally published in 1942 and deduced from Weissenberg photographs. We have discussed the Bi/Pb segregation in the several building units, and finally we propose an ideal model with preferred sites for Pb^{2+} at the origin of the general formula given above. This work represents a new example of megaseries that pave the future of inorganic chemistry toward a rational understanding of solids. Moreover, these compounds are very promising due to their outstanding luminescent properties, and their investigations will lead to a contribution to the understanding to the structure−luminescence relationship of s^2 ions, which are suitable candidates for the substitution of lanthanide ions in phosphors for saving recourses.

ASSOCIATED CONTENT

Supporting Information

Additional tables. This material is available free of charge via the Internet at http://pubs.acs.org.

AUTHOR INFORMATION

Corresponding Author

*E-mail: olivier.mentre@ensc-lille.fr.

dx.doi.org/10.1021/ic4002708 | Inorg. Chem. 2013, 52, 8427−8435

Notes

The authors declare no competing financial interest.

REFERENCES

(1) Blasse, G.; Sytsma, J.; Brixner, L. H. *Chem. Phys. Lett.* **1989**, *155*, 64−68.
(2) Wu, S.; Wang, C.; Cui, Y.; Wang, T.; Huang, B.; Zhang, X.; Qin, X.; Brault, P. *Mater. Lett.* **2010**, *64*, 115−118.
(3) Hessel, C. M.; Reid, D.; Panthani, M. G.; Rasch, M. R.; Goodfellow, B. W.; Wei, J.; Fujii, H.; Akhavan, V.; Korgel, B. A. *Chem. Mater.* **2012**, *24*, 393−401.
(4) Nguyen, S. D.; Yeon, J.; Kim, S.-H.; Halasyamani, P. S. *J. Am. Chem. Soc.* **2011**, *133*, 12422−12425.
(5) Smirnova, O.; Azuma, M.; Kumada, N.; Kusano, Y.; Matsuda, M.; Shimakawa, Y.; Takei, T.; Yonesaki, Y.; Kinomura, N. *J. Am. Chem. Soc.* **2009**, *131*, 8313−8317.
(6) Endara, D.; Colmont, M.; Huvé, M.; Capet, F.; Lejay, J.; Aschehoug, P.; Mentré, O. *Inorg. Chem.* **2012**, *51*, 9557−9562.
(7) Huvé, M.; Colmont, M.; Lejay, J.; Aschehoug, P.; Mentré, O. *Chem. Mater.* **2009**, *21*, 4019−4029.
(8) Cornei, N.; Tancret, N.; Abraham, F.; Mentré, O. *Inorg. Chem.* **2006**, *45*, 4886−4888.
(9) Krivovichev, S. V.; Mentré, O.; Siidra, O. I.; Colmont, M.; Filatov, S. K. *Chem. Rev.* **2013**, DOI: DOI: 10.1021/cr3004696.
(10) Arppe, A. E. *Ann. Phys. Chem.* **1845**, *140*, 237−251.
(11) Sillen, L. G.; Edstrand, M. *Z. Kristallogr.* **1942**, *104*, 178−196.
(12) Eggenweiler, U.; Keller, E.; Krämer, V. *Acta Crystallogr., Sect. B* **2000**, *56*, 431−437.
(13) Siidra, O. I.; Krivovichev, S. V.; Armbruster, T.; Depmeier, W. *Inorg. Chem.* **2007**, *46*, 1523−5.
(14) Belokoneva, E. L.; Dimitrova, O. V. *Crystallogr. Rep.* **2010**, *55*, 24−27.
(15) Siidra, O. I.; Krivovichev, S. V.; Armbruster, T.; Depmeier, W. *Z. Kristallogr.* **2008**, *223*, 204−211.
(16) Siidra, O. I.; Krivovichev, S. V.; Depmeier, W. *Dokl. Phys. Chem.* **2007**, *414*, 128−131.
(17) Berdonosov, P. S.; Charkin, D. O.; Dolgikh, V. A.; Popovkin, B. A. *Russ. J. Inorg. Chem.* **1999**, *44*, 1031−1037.
(18) Sillén, L. G. *Z. Anorg. Allg. Chem.* **1939**, *242*, 41−46.
(19) Sillén, L. G. *Naturwissenschaften* **1942**, *30*, 318−324.
(20) Gilberg, M. *Ark. Kemi, Mineral. Geol.* **1960**, *B2*, 565.
(21) Kirik, S. D.; Yakovleva, E. G.; Shimanskii, A. F.; Kovalev, Y. G. *Acta Crystallogr., Sect. C* **2001**, *57*, 1367−1368.
(22) Fray, S. M.; Milne, C. J.; Lightfoot, P. *J. Solid State Chem.* **1997**, *128*, 115−120.
(23) Keramidas, K. G.; Voutsas, G. P.; Rentzeperis, P. I. *Z. Kristallogr.* **1993**, *205*, 35−40.
(24) Lopatin S, S. *Zh. Neorg. Khim.* **1987**, *32*, 1694−1697.
(25) Dolgikh, V. A.; Kholodkovskaya, L. N. *Russ. J. Inorg. Chem.* **1992**, *37*, 488.
(26) Ketterer, J.; Krämer, V. *Mater. Res. Bull.* **1985**, *20*, 1031−1036.
(27) Deschanvres, A.; Gallay, J.; Hunout, J.-M.; Thiault, M.-T.; Victor, C. *C. R. Acad. Sci. Paris* **1970**, *270*, 696.
(28) Kennard, M. A.; Darriet, J.; Grannec, J.; Tressaud, A. *J. Solid State Chem.* **1995**, *117*, 201−205.
(29) *SAINT: Area-Detector Integration Software*; Siemens Industrial Automation, Inc.: Madison, WI, 1996.
(30) *SADABS: Area-Detector Absorption Correction*; Siemens Industrial Automation, Inc.: Madison, WI, 1995.
(31) Rodriguez-Carvajal, J. *Recent Developments of the Program FULLPROF*; 2001.
(32) Aurivillius, B. *Chem. Scr.* **1987**, *27*, 397−402.
(33) Krivovichev, S. V.; Filatov, S. K. *Crystal chemistry of minerals and inorganic compounds with complexes of anion-centered tetrahedra*; St. Petersburg University Press: St. Petersburg, 2001.
(34) Kozin, M. S.; Aliev, A.; Colmont, M.; Mentré, O.; Siidra, O. I.; Krivovichev, S. V. *J. Solid State Chem.* **2013**, *199*, 56−61.
(35) Schmidt, M.; Oppermann, H.; Hennig, C.; Henn, R. W.; Gmelin, E.; Söger, N.; Binnewies, M. *Z. Anorg. Allg. Chem.* **2000**, *626*, 125−135.
(36) Brese, N. E.; O'Keeffe, M. *Acta Crystallogr., Sect. B* **1991**, *47*, 192−197.
(37) Krivovichev, S. V. *Z. Kristallogr.—Cryst. Mater.* **2012**, *227*, 575−579.
(38) Rolle, A.; Preux, N.; Ehora, G.; Mentré, O.; Daviero-Minaud, S. *Solid State Ionics* **2011**, *184*, 31−34.
(39) Okamoto, K.; Imanaka, N.; Adachi, G. *Solid State Ionics* **2002**, *154−155*, 577−580.
(40) Folkerts, H. F.; Zuidema, J.; Blasse, G. *Chem. Phys. Lett.* **1996**, *249*, 59−63.
(41) Manavbasi, A.; LaCombe, J. C. *J. Lumin.* **2008**, *128*, 129−134.
(42) Van de Craats, A. M.; Dirksen, G. J.; Blasse, G. *J. Solid State Chem.* **1995**, *118*, 337−340.
(43) Blasse, G. *Prog. Solid State Chem.* **1988**, *18*, 79−171.
(44) Duffy, J. A.; Ingram, M. D. *J. Chem. Phys.* **1970**, *52*, 3752−3754.
(45) Boulon, G.; Moine, B.; Bourcet, J. C.; Reisefeld, R.; Kalisky, Y. *J. Lumin.* **1979**, *18−19* (Part 2), 924−928.
(46) Sidike, A.; Wang, X.-M.; Sawuti, A.; Zhu, H.-J.; Kusachi, I.; Yamashita, N. *Phys. Chem. Miner.* **2006**, *33*, 559−566.
(47) Srivastava, A. M.; Beers, W. W. *J. Lumin.* **1999**, *81*, 293−300.
(48) Timmermans, C. W. M.; Blasse, G. *J. Solid State Chem.* **1984**, *52*, 222−232.
(49) Parke, S.; Webb, R. S. *J. Phys. Chem. Solids* **1973**, *34*, 85−95.
(50) Xu, W.; Peng, M.; Ma, Z.; Dong, G.; Qiu, J. *Opt. Express* **2012**, *20*, 15692−15702.
(51) Cao, R.; Peng, M.; Wondraczek, L.; Qiu, J. *Opt. Express* **2012**, *20*, 2562−2571.
(52) Hamstra, M. A.; Folkerts, H. F.; Blasse, G. *J. Mater. Chem.* **1994**, *4*, 1349−1350.
(53) Peng, M.; Wondraczek, L. *J. Am. Ceram. Soc.* **2010**, *93*, 1437−1442.